Creation of multiple identical single photon emitters in diamond

L. J. Rogers,[1] K. D. Jahnke,[1] L. Marseglia,[1] C. Müller,[1] B. Naydenov,[1] H. Schauffert,[1] C. Kranz,[2] T. Teraji,[3] J. Isoya,[4] L. P. McGuinness,[1] and F. Jelezko[1]

[1] *Institute for Quantum Optics and Center for Integrated Quantum Science and Technology (IQst), University Ulm, D-89081 Germany*
[2] *Institute of Analytical and Bioanalytical Chemistry, University Ulm, D-89081 Germany*
[3] *National Institute for Materials Science, 1-1 Namiki, Tsukuba, Ibaraki 305-0044, Japan*
[4] *Research Center for Knowledge Communities, University of Tsukuba, 1-2 Kasuga, Tsukuba, Ibaraki 305-8550, Japan*

Emitters of indistinguishable single photons are crucial for the growing field of quantum technologies. To realize scalability and increase the complexity of quantum optics technologies, multiple independent yet identical single photon emitters are also required. However typical solid-state single photon sources are dissimilar, necessitating the use of electrical feedback or optical cavities to improve spectral overlap between distinct emitters. Here, we present controllable growth of bright silicon-vacancy (SiV^-) centres in bulk diamond which intrinsically show almost identical emission (spectral overlap of up to 83%) and near transform-limited excitation linewidths. We measure the photo-physical properties of defects at room and cryogenic temperatures, and demonstrate incorporation into a solid immersion lens (SIL). Our results have impact upon the application of single photon sources for quantum optics and cryptography, and the production of next generation fluorophores for bio-imaging.

Single, transform-limited photons are an essential resource for many quantum interference experiments, since indistinguishability between photons allows the path-of-origin information to be erased. This makes possible investigations of fundamental quantum optics phenomena which have applications in quantum imaging [1], quantum computing [2] and quantum repeaters [3]. Interactions between indistinguishable photons from multiple emitters can also be used to create entangled quantum states over macroscopic physical distances [4]. Moreover, deterministic scaling to higher numbers of entangled photon states can be achieved by using several identical emitters. However, to date it has proved difficult to achieve indistinguishability between distinct single photon sources.

Quantum dots have demonstrated transform-limited linewidths over short timescales, allowing interference between photons from the same emitter[5] and physically separated defects [6]. Single molecules embedded in a matrix have also been used to demonstrate two photon interference [7], but with the exception of trapped ions in vacuum [8], it has been necessary to use optical cavities and/or electrical tuning in order to interfere photons from distinct emitters [9]. In contrast, diamond-based colour centres, located deep within an ultra-pure lattice show excellent photostability, and unlike trapped ions, allow for direct incorporation into photonic and plasmonic devices. Currently, the negative nitrogen vacancy (NV^-) centre is the favoured emitter [10, 11], despite the spectral properties of NV^- being ill-suited to single photon technologies and two photon interference [4]. A number of potential alternate colour centres in diamond have also been reported [12–14] including the negative silicon-vacancy (SiV^-) centre [15–17]. The SiV^- defect is understood to be comprised of a silicon atom located between adjacent vacancies in the diamond lattice [16, 18, 19] (Figure 1(a). It is associated with a strong optical transition with a prominent zero-phonon line (ZPL) at 738.4 nm and only a weak phonon sideband [20–24]. These properties have sparked interest, but large variation in spectral properties between individual sites has limited the value of SiV^- as a single photon emitter.

In these experiments we obtained highly uniform, narrow linewidths by using low strain, high-pressure, high-temperature (HPHT) diamonds as substrates due to their high crystalline quality. A layer of ultrapure diamond with silicon concentration below 1 ppb, was grown on the $\langle 100 \rangle-$oriented substrate with microwave-plasma chemical-vapour deposition (CVD), allowing precise control of impurity concentrations. Single fluorescent SiV^- defects could then be observed by fluorescence confocal microscopy (Figure 1(b,c). First we describe the optical properties of single sites measured at room-temperature. Photon antibunching measurements provided confirmation of single photon emission, and pulsed excitation gave an excited-state lifetime of 1.0 ± 0.1 ns (Figure 1(d). The excitation power was varied to measure the SiV^- fluorescence saturation, with the maximum count rate of 277 kcts/sec comparable to a single NV^- centre or bright molecule (Figure 1(e). The fluorescence polarisation was also investigated (see Methods), and two orientations were observed, offset by 90° (Figure 1(f). We obtain an polarisation visibility of 0.60 ± 0.05 in $\langle 100 \rangle-$oriented diamond, which can be improved by orienting the viewing angle with respect to the dipole axis [25]. Every individual emitter (N = 28) showed identical properties, within stated uncertainties.

The spectral properties of individual centres were then recorded using 532 nm excitation, and a typical spectrum is shown in Figure 2(a). The ZPL position of 738.4 ± 0.05 nm and spectral linewidth of 4.6 ± 0.2 nm were also identical for every centre within the spectrometer resolution. The linewidth is amongst the narrowest of any solid state emitter at room temperature. The nar-

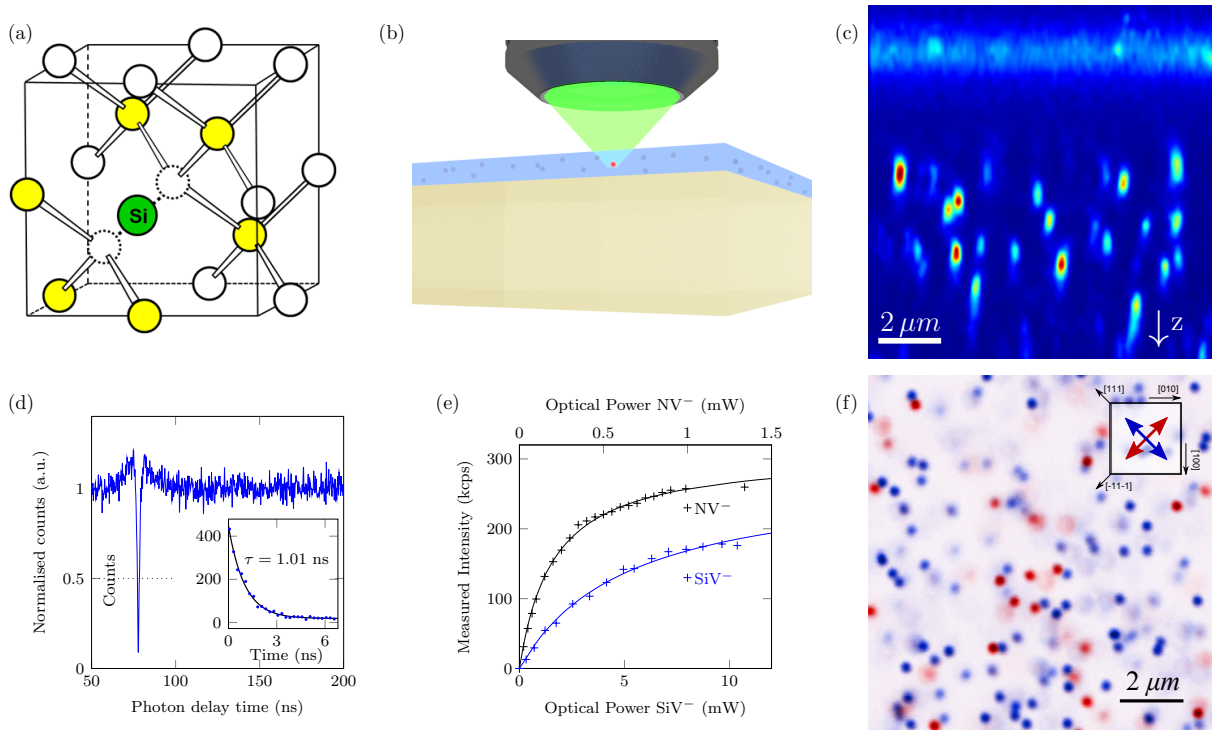

FIG. 1. Single photon emitters with uniform properties in diamond. (a) Physical structure of the SiV^- centre in the diamond lattice. (b) Single crystal CVD diamond layers, doped with silicon to create SiV^- centres were grown homoepitaxially on low strain, high-pressure, high-temperature diamond substrates and investigated from the top. (c) Fluorescence confocal image showing the depth profile of single SiV^- centres, grown in the CVD diamond layer. (d) Photon $g_2(\tau)$ correlation function from single centres demonstrating single photon emission. (Inset) Pulsed lifetime measurements gave an excited state lifetime of $\tau = 1.0 \pm 0.1$ ns at room temperature. (e) Fluorescence intensity saturation plot from a single SiV^- defect at room temperature with detected fluorescence saturating above 277,000 counts/sec and compared with the fluorescence from a single NV^- defect. Optical power is given as the power measured at the back aperture of the objective (Olympus UPLSAPO, 60× 1.35 N.A.). (f) Confocal image 5 microns into the diamond, showing orientation of fluorescence polarisation from single silicon-vacancy centres. Colour encodes the polarisation direction, as indicated by the arrows.

row linewidth is advantageous for biolabelling to allow improved multicolor imaging without crosstalk between fluorophores. Also of significance is that the majority of the fluorescence lies in the zero phonon line, rather than the phonon sidebands (Debye-Waller factor = 70%) making this centre ideal for coupling to narrowband cavities and single photon interference experiments including quantum cryptography.

To investigate the emission spectrum with higher resolution, the sample was cooled below 10 K in a continuous flow helium cryostat. As the temperature is decreased the ZPL shifts to shorter wavelengths as shown in Figure 2(a) [26]. Although the sideband features are much sharper at cryogenic temperatures, they do not gain significantly in intensity relative to the ZPL (Debye-Waller = 64%). The sideband was identical for all measured sites.

The ZPL consists of four lines, and these were measured in photoluminescence excitation (PLE) using a resonant laser with 50 kHz linewidth. The spectrum for a single emitter is shown in Figure 2(b). The pair of lines at longer wavelength (lowest energy) have a linewidth of 230 ± 20 MHz, which is close to the expected lifetime-limited value [26]. The higher energy pair of lines have a width of 610 ± 20 MHz. Low temperature photoluminescence measurements show that for equivalent transition dipoles, the higher energy line has a weaker emission than the lower energy line (Figure 2(c), but at temperatures above 50 K both lines have similar intensity. This is a result of thermalisation in the SiV^- excited state. Relaxation from the upper branch as illustrated in Figure 2(d) provides an additional decay channel, whereas at low temperature the thermal energy is insufficient to overcome the excited state energy splitting so the reverse process does not occur. This extra one-way transition from the excited state upper branch reduces the effective lifetime of the shorter wavelength lines, causing the lower energy lines to be broader and reducing their intensity.

Over a period of 90 minutes the line position of one defect was recorded (Figure 3(a), and remarkably no spectral diffusion was observed, highlighting the stability of this emitter and indicating that indistinguishable photons can be produced over long periods. Additional comparison of the spectrum for five sites gave a variation in

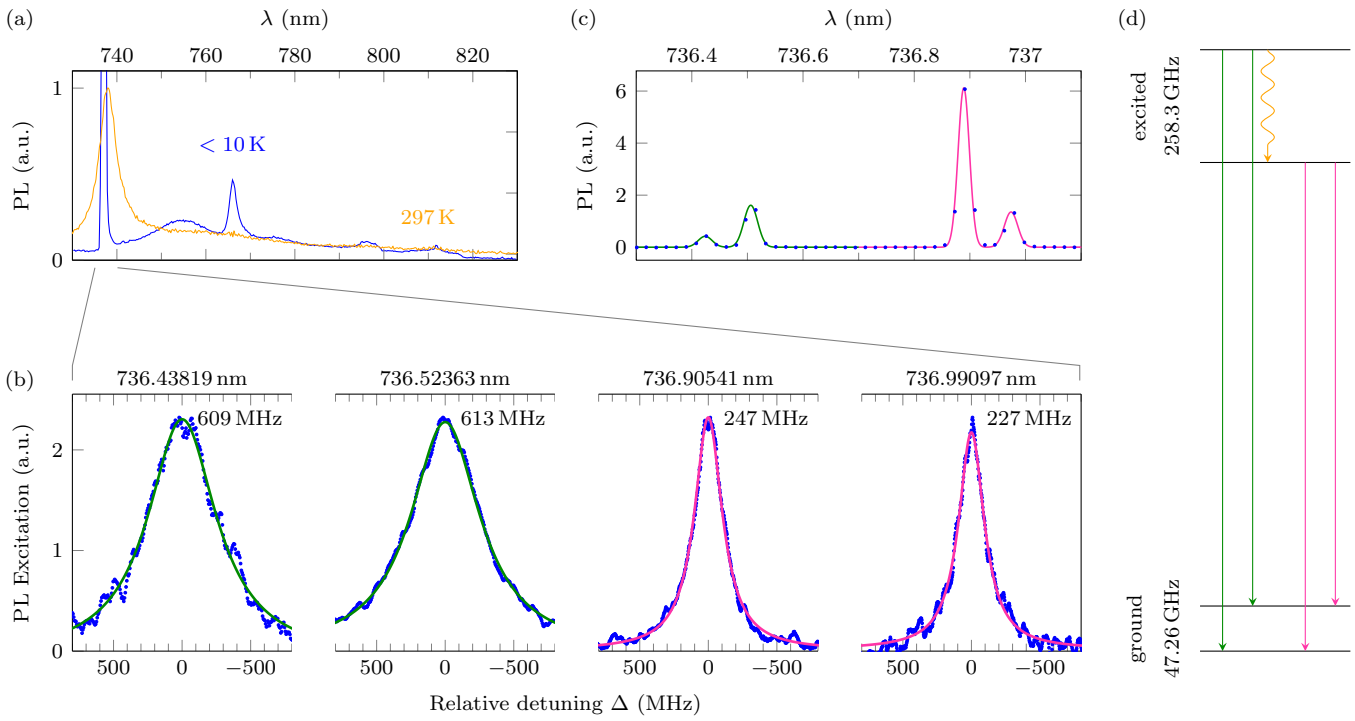

FIG. 2. Overview of spectral properties. (a) Typical photoluminescence spectra from a single SiV^- site at room (pink) and cryogenic (blue) temperatures. The sideband contains peaks redshifted from the ZPL by 41, 64, 84, 128, and 152 meV. There was no measurable variation across the band between sites. (b) Excitation specta of the four lines that comprise the SiV^- ZPL (amplitudes normalised). The higher energy lines are wider, consistent with a shorter effective lifetime due to thermalisation between the two excited state branches. (c) Polarisation-independent PL spectrum from the same SiV^- site at low temperature (linewidth limited by spectrometer resolution). Comparison of the intensity of the inner pair of lines, which correspond to transitions between states of same symmetry, gives an intensity of the longer wavelength line about 3.5 times that of the shorter wavelength, but this difference disappears as the temperature increases (similarly when comparing the outer pair of lines). (d) Basic SiV^- energy scheme. The excited state splitting is large enough for one-way thermalisation to occur between the two branches at low temperature, effectively reducing the lifetime of the upper branch.

line position of 109 MHz, well below the linewidth (Figure 3(b). Even in this small sample size, spectral overlap between emitters as high as 83% was observed, which is important for high success rate two-photon interference experiments between multiple emitters. Notably, nearly complete spectral overlap was achieved without external tuning of the spectral position.

To explain the observed homogeneity, we return briefly to the four line structure seen in Figure 2(c), consistent with transitions between two states of E symmetry [16, 25]. The ground and excited state splittings illustrated in Figure 2(d) are understood to result from spin-orbit interaction [25]. They are large for spin-orbit (an order of magnitude higher than NV^-), which would make the SiV^- centre unresponsive to small strains and electric fields and may explain the extreme uniformity. Separate measurements on defects in a ⟨111⟩ growth sector of HPHT diamond, known to have higher strain than ⟨100⟩ sectors, showed a variation in line position an order of magnitude greater than this, indicating that the high quality CVD crystals used in these experiments were also crucial to obtaining uniform spectra.

We have produced single photon emitters without site-to-site variation in wavelength, an important benchmark for enabling efficient co-operation with photonic cavities [27]. We now show incorporation into a photonic structure, demonstrating their readiness for applications in quantum optics experiments. We use a SIL as a test case, since they are useful for outcoupling light from high index materials [28]. Of particular significance is their use in cryogenic experiments, where oil-immersion is not possible.

Positioning of emitters near the SIL focus was achieved statistcally by creating an array of 20 SILs (of which one is shown in Figure 4(a) on a diamond with an increased density of SiV^- centers. Well coupled SiV^- centres were identified by scanning the depth profile with a confocal microscope (Figure 4(c). Each SIL contained several defects with various fluorescence intensity depending on their position relative to the SIL focus. In Figure 4(b), the simulated emitted field intensity for a defect at the focus depicts how the SIL acts to reduce total internal reflection and enhance fluorescence collection. Fluorescence from a single site, confirmed with photon

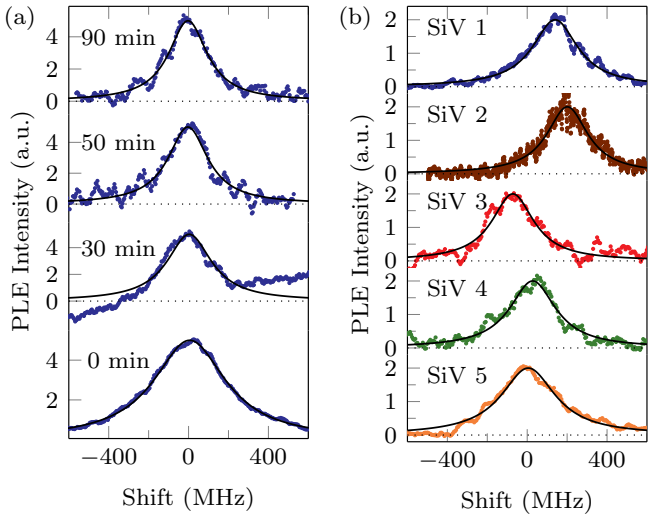

FIG. 3. Long term stability and uniformity of single SiV$^-$ centres. (a) The excitation spectrum of a single emitter with 250 ± 20 MHz linewidth was investigated over 90 minutes and showed no variation in spectral position over the investigated time (amplitudes are normalised). (b) High resolution excitation spectra of five randomly selected sites showing an average linewidth of 280 ± 30 MHz and a site-to-site deviation of 109 MHz (amplitudes are normalised). The lowest two curves have an overlap of 83% and the overlap of all five sites is 27%.

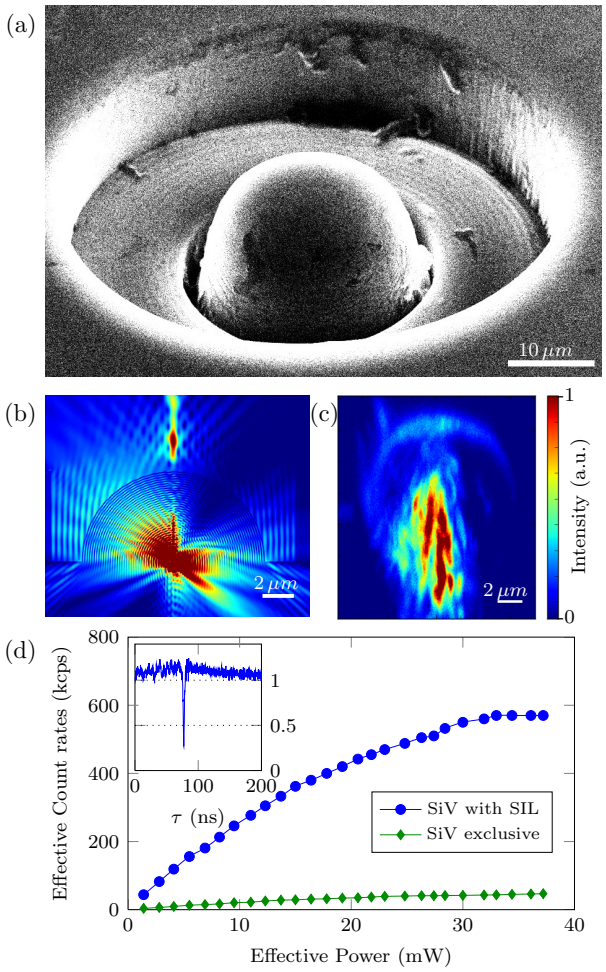

FIG. 4. SiV$^-$ incorporation into a SIL. (a) Scanning electron microscope image of a single SIL fabricated in the diamond surface, taken with a Helios Nanolab 600 Focussed Ion Beam lithography system. (b) Simulation of the emission intensity for a single dipole located at the centre of the solid immersion lens. Calculated with finite-difference time-domain numerical package. (c) Cross-section of fluorescence intensity profile from a SIL, showing enhanced fluorescence detection for SiV$^-$ centres near the focus. (d) Comparision of the total count-rate for SiV$^-$ under SIL with a single SiV$^-$ under a planar surface nearby, shown as a function of excitation power. The SIL gives a 10× enhancement in detected counts. (Inset) Measurement of the $g_2(\tau)$ correlation function for the same centre providing the data in the main figure. The dip reaching below 0.5 shows that the majority of the fluorescence comes from this center.

antibunching (see Figure 4(d inset) was measured for increasing excitation intensity, and was found to saturate at nearly 600 kcts/sec, compared to only 60 kcts/sec without the SIL (Figure 4(d), providing an enhanced photon collection by a factor of ten. Despite using an air objective with much lower numerical aperture, the saturated count-rate from the SiV$^-$ coupled to the SIL was double that of an isolated site imaged with an oil-immersed objective.

In summary, we have demonstrated a uniform single photon source in diamond with desirable properties. In particular, at room-temperature are high brightness emission at near-infrared wavelength into a narrow band and with well-defined polarisation. Applications include quantum key distribution and coupling to photonic devices, where we have shown that the SiV$^-$ may be readily incorporated into a solid immersion lens. The near-infrared emission means that higher Q factor structures are more readily achieved and the propagation length for surface plasmons is increased when compared to the visible range. For bio-imaging applications, near-infrared fluorescence also allows for deep tissue imaging and results in lower autofluorescence.

At low temperature we observe near lifetime-limited excitation linewidths, without spectral diffusion, allowing almost spectral overlap between subsequent single photons emitted from the same source, for times exceeding an hour. The SiV$^-$ centre is therefore promising for applications requiring the generation of individual photons into a single radiative mode. We also obtain a variation in excitation spectra for multiple emitters of less than 20%. The production of multiple, independent single photon emitters with identical properties, is essential to the scalability of a number of schemes that utilise entangled photons, including quantum computing with linear optics, and is expected to form a fundamental resource in quantum optics technologies.

ACKNOWLEDGEMENTS

We acknowledge ERC, DFG (FOR 1482, FOR 1493 and SFBTR 21), JST, and the Alexander von Humboldt, Sino-German and Volkswagen foundations for funding. We acknowledge G. Neusser and the FIB Center UUlm for support manufacturing SILs.

SUPPLEMENTARY MATERIAL

Sample preparation

⟨100⟩−oriented plates cut from a low-strain, type-IIa, HPHT crystal (Sumitomo Electric Industries, Ltd.) were used as a substrate. High-purity H_2 and CH_4 source gas, specified to 99.999% 12C isotopic enrichment (Cambridge Isotope Laboratories CLM-392), with residual N_2 concentration less than 0.1 ppb for H_2 and less than 1 ppb for CH_4 was used. The total gas pressure, microwave power, methane concentration ratio (CH_4/ H_2), growth duration and substrate temperature employed were 120 Torr, 1.4 kW, 4 %, 24 h, and 950 – 1000 °C, respectively. The homoepitaxial layer thickness estimated from the weight difference between initial substrate and after the growth was $\sim 60\,\mu$m. Thereby the growth rate in this condition is $2.4\,\mu$m/h. Cathodoluminescence spectra (15 kV acceleration voltage, 2×10^{-7}A incident beam current) taken at room temperature in a wavelength range from 200 – 800 nm provided information on the crystalline quality and optically active impurities. Emission from free-exciton recombination was intensely observed from the most of the growth surface, in addition to a weak signal at 738 nm, being assigned as SiV^-. The reaction vessel of MPCVD contains mainly stainless steel and molybdenum. Si containing materials such as silica glass (SiO_2) are used for the windows of the vessel. When homoepitaxial film was grown under the low microwave power, no SiV^- fluorescence was observed. By increasing the microwave input power, the incorporation of SiV^- below $0.2/\,\mu m^3$ ($\sim 1 \times 10^{-3}$ppb) could be produced, as shown in Figure 1(a). Incorporation of silicon occurred relatively uniformly over the whole lateral direction. The SiV- concentration could be varied to a factor of thousand by putting Si containing material.

Optical measurements

The confocal images at room temperature were taken by scanning the position of a 532 nm laser focused into the diamond using a 1.35 N.A. oil-immersion objective. Fluorescence was collected by the same objective, filtered with a 725–775 nm band-pass filter before detection with an avalanche photodiode. At cryogenic temperatures a 0.95 N.A. air objective was used. By rotating a half-wave plate in the collection arm of the confocal microscope the polarisation dependence of defects was recorded (see supplementary video).

A spectrometer also in the detection arm was used to acquire spectra from single sites. Using a high resolution grating (1596 lines per inch) allowed four component lines comprising the ZPL to be resolved. Fits were applied for each line at each site in order to more reliably obtain the position and width. Across this large sample set the standard deviation in line position was less than 2 GHz, but the instrument limited linewidths prevented identification of the actual variation in line position.

SIL fabrication

In a sample known to contain a medium density of SiV^- centres at a depth of 2.5-6 μm below the surface, the SILs were produced. The site density was high enough to assure a high probability of coupling a SIL to a colour centre. The fabrication process was performed with Helios Nanolab 600 Focus Ion Beam (FIB) lithography system. Each SIL had a radius of 7 μm and a depth of 7 μm.

REFERENCES

[1] D. Strekalov, A. Sergienko, D. Klyshko, and Y. Shih, Physical Review Letters **74**, 3600 (1995).

[2] E. Knill, R. Laflamme, and G. J. Milburn, Nature **409**, 46 (2001).

[3] Z.-S. Yuan, Y.-A. Chen, B. Zhao, S. Chen, J. Schmiedmayer, and J.-W. Pan, Nature **454**, 1098 (2008).

[4] H. Bernien, B. Hensen, W. Pfaff, G. Koolstra, M. Blok, L. Robledo, T. Taminiau, M. Markham, D. Twitchen, and L. Childress, Nature **497**, 86 (2013).

[5] C. Santori, D. Fattal, J. Vuckovic, G. S. Solomon, and Y. Yamamoto, Nature **419**, 594 (2002).

[6] R. B. Patel, A. J. Bennett, I. Farrer, C. A. Nicoll, D. A. Ritchie, and A. J. Shields, Nature Photonics **4**, 632 (2010).

[7] A. Kiraz, M. Ehrl, T. Hellerer, O. E. Müstecaplıoğlu, C. Bräuchle, and A. Zumbusch, Physical Review Letters **94**, 223602 (2005).

[8] J. Beugnon, M. P. Jones, J. Dingjan, B. Darquié, G. Messin, A. Browaeys, and P. Grangier, Nature **440**, 779 (2006).

[9] A. J. Shields, Nature Photonics **1**, 215 (2007).

[10] A. Faraon, C. Santori, Z. Huang, V. M. Acosta, and R. G. Beausoleil, Physical Review Letters **109**, 033604 (2012).

[11] P. E. Barclay, K.-M. C. Fu, C. Santori, A. Faraon, and R. G. Beausoleil, Physical Review X **1**, 011007 (2011).

[12] S. Castelletto, J. P. Harrison, L. Marseglia, A. C. Stanley-Clarke, B. C. Gibson, B. A. Fairchild, J. P. Hadden, Y.-L. D. Ho, M. P. Hiscocks, K. Ganesan, S. T. Huntington, F. Ladouceur, A. D. Greentree, S. Prawer, J. L. O'Brien, and J. G. Rarity, New Journal of Physics **13**, 025020 (2011).

[13] T. Gaebel, I. Popa, A. Gruber, M. Domhan, F. Jelezko, and J. Wrachtrup, New J. Phys. **6**, 98 (2004).

[14] S.-Y. Lee, M. Widmann, T. Rendler, M. W. Doherty, T. M. Babinec, S. Yang, M. Eyer, P. Siyushev, B. J. M. Hausmann, M. Loncar, Z. Bodrog, A. Gali, N. B. Manson, H. Fedder, and J. Wrachtrup, Nature Nanotechnology **8**, 487 (2013).

[15] A. T. Collins, M. Kamo, and Y. Sato, Journal of Materials Research **5**, 2507 (1990).

[16] J. P. Goss, R. Jones, S. J. Breuer, P. R. Briddon, and S. Öberg, Physical Review Letters **77**, 3041 (1996).

[17] G. Sittas, H. Kanda, I. Kiflawi, and P. Spear, Diamond and Related Materials **5**, 866 (1996).

[18] A. V. Turukhin, C.-H. Liu, A. A. Gorokhovsky, R. R. Alfano, and W. Phillips, Physical Review B **54**, 16448 (1996).
[19] C. Wang, C. Kurtsiefer, H. Weinfurter, and B. Burchard, Journal of Physics B: Atomic, Molecular and Optical Physics **39**, 37 (2006).
[20] T. Feng and B. D. Schwartz, Journal of Applied Physics **73**, 1415 (1993).
[21] E. Neu, D. Steinmetz, J. Riedrich-Mller, S. Gsell, M. Fischer, M. Schreck, and C. Becher, New Journal of Physics **13**, 025012 (2011).
[22] S. W. Brown and S. C. Rand, Journal of Applied Physics **78**, 4069 (1995).
[23] C. D. Clark, H. Kanda, I. Kiflawi, and G. Sittas, Physical Review B **51**, 16681 (1995).
[24] A. M. Edmonds, M. E. Newton, P. M. Martineau, D. J. Twitchen, and S. D. Williams, Physical Review B **77**, 245205 (2008).
[25] L. J. Rogers, K. D. Jahnke, M. W. Doherty, A. Dietrich, L. McGuinness, C. Mller, T. Teraji, J. Isoya, N. B. Manson, and F. Jelezko, In Preparation **0**, 0 (2013).
[26] E. Neu, C. Hepp, M. Hauschild, S. Gsell, M. Fischer, H. Sternschulte, D. Steinmller-Nethl, M. Schreck, and C. Becher, New Journal of Physics **15**, 043005 (2013).
[27] I. Aharonovich, A. Greentree, and S. Prawer, Nature Photonics **5**, 397 (2011).
[28] L. Marseglia, J. P. Hadden, A. C. Stanley-Clarke, J. P. Harrison, B. Patton, Y.-L. D. Ho, B. Naydenov, F. Jelezko, J. Meijer, P. R. Dolan, J. M. Smith, J. G. Rarity, and J. L. OBrien, Applied Physics Letters **98**, 133107 (2011).